Journal of Hydrology: Regional Studies 50 (2023) 101599

Contents lists available at ScienceDirect

Journal of Hydrology: Regional Studies

journal homepage: www.elsevier.com/locate/ejrh

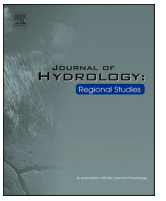

Importance of small geological features for simulated spatial patterns in tile drain flow in Fensholt catchment of Denmark

Hafsa Mahmood [a,*], Rasmus Rumph Frederiksen [b], Carlos Duque [c], Anders Vest Christiansen [a]

[a] Department of Geoscience, Aarhus University, 8000 Aarhus, Denmark. Also affiliated with WATEC, Aarhus University Centre for Water Technology (watec.au.dk), Denmark
[b] Department of Ecoscience, Aarhus University, Aarhus 8000, Denmark
[c] Department of Geodynamics. University of Granada, Spain

ARTICLE INFO

Keywords:
Subsurface drainage
Geophysical mapping
Geological model
Groundwater model
Topographical index

ABSTRACT

Study region: Fensholt, Denmark.
Study focus: Tile drains are commonly used in agricultural fields with loamy soils in Denmark to improve crop yield by removing excessive water. Spatial patterns of drain flows are controlled by the climate, geology, topography, and tile installation. We assessed the combined effect of topography and geology on spatial pattern of tile drain flows in 10 m resolution using numerical modelling. We developed three groundwater models using different geological models by integrating high-resolution data from geophysical methods with field estimated hydraulic conductivity.
New insights: The mapping and modelling revealed small geological features of higher hydraulic conductivity in clayey-till. The results showed that the spatial patterns of drain flows to recharge ratio (drainage fraction, DF) are driven by topography; the models had a high DF in local depressions and a low DF in local hills. The DF was related to the Topographical Position Index (TPI), suggesting that the DF is controlled by small-scale topography both upstream and downstream of the study area. We found that geology amplifies the spatial patterns of tile drain flows; a higher hydraulic conductivity relative to a lower hydraulic conductivity increases the change of tile drain flow for a one-unit change in the TPI. This was attributed to a change from small-scale flow systems to field-scale flow systems. The study suggested that topography helps to delineate high and low DF while geology controls the magnitude of DF. The study emphasized the importance of mapping and modeling of geology for managing moraine agricultural areas that can be found in parts of North America and Scandinavia for agricultural water management.

1. Introduction

Tile drainage systems consist of underground networks of perforated pipes that are used to remove excess water from agricultural fields to increase crop growth and soil health (Williamson and Kriz, 1970; Zucker and Brown, 1998). In Denmark, around 50 % of agricultural land is tile drained with a typical tile depth and spacing of 0.7–1.2 m and 20 m (Nielsen, 2015), respectively. Tile drains

* Corresponding author.
E-mail address: hm@geo.au.dk (H. Mahmood).

https://doi.org/10.1016/j.ejrh.2023.101599
Received 19 May 2023; Received in revised form 29 November 2023; Accepted 2 December 2023
Available online 7 December 2023

not only play a critical role in regulating the hydrology at the field scale, but they can also significantly impact water quantity and quality at the watershed scale. For example, tile drains shorten the travel time in the subsurface, and increase the water volumes and nutrient loads to streams (Boland-Brien et al., 2014; Clement and Steinman, 2017; Schilling et al., 2012; Schilling et al., 2020) which can lead to downstream flooding and issues with the water quality like eutrophication (Clement and Steinman, 2017; Sloan et al., 2017). Thus, a better understanding and quantification of groundwater discharge to tile drains at the field scale is important to water managers for sustainable water resource management and to prevent water quality deterioration.

Haitjema and Mitchell-Bruker (2005) and Anderson et al. (2015) concluded that the groundwater tables are either recharge or topography controlled. Topography-controlled water tables are associated with low-permeable or anisotropic aquifers in regions with high recharge rates or flat terrain, while recharge-controlled aquifers are relatively permeable with an average recharge (Haitjema and Mitchell-Bruker, 2005). However, the objectives of these past studies were to understand the control of topography on groundwater levels and did not include studying the implications of tile drain flow generation.

Tile drain flow generation is variable across both time and space controlled by a range of complex processes governed by topography (Hansen et al., 2019a; Mahmood et al., 2023; Motarjemi et al., 2021), geology (Hansen et al., 2019a), climate (Frederiksen et al., 2023; Kladivko et al., 2004; Motarjemi et al., 2021), and tile installation (Kladivko and Bowling, 2021; Sinai and Jain, 2005). While many past studies have investigated the control of the drainage system design (Helmers et al., 2022; Kladivko and Bowling, 2021; Kladivko et al., 2004; Ross et al., 2016; Sinai and Jain, 2005) and climatic factors (Helmers et al., 2022; Kladivko and Bowling, 2021; Kladivko et al., 2004) on tile drain flows, the impact of field hydrology and field characteristics such as hydraulic conductivity and topography are less explored (Ross et al., 2016).

Among the studies concerning the impact of field characteristics on tile drain flow, most researchers have investigated either impacts of field characteristics on only the temporal dynamics of tile drain flow (De Schepper et al., 2017; Hansen et al., 2019b; Motarjemi et al., 2021), or the impacts of tile drains on hydrological fluxes in shallow depths (Hansen et al., 2019b). However, correlation of spatial tile drain flows with spatially distributed topography and hydraulic conductivity are not studied extensively. Motarjemi et al. (2021) examined the correlation of topographic indexes (TI) such as the topographical wetness index (TWI). However, the authors were unsuccessful in finding a correlation of catchment average TI and annual average tile drain flows for multiple field scale catchments, because spatial differences of TI and tile drain flows were not considered. Hansen et al. (2019a) considered spatial distribution of TWI and tile drain flows for correlation analysis, but found a weak correlation because a low spatial model resolution (of 100 m) was not enough to capture the tile drain flow patterns on field scale. Boico et al. (2022) studied the impact of geological heterogeneity on the tile drain flow temporal and spatial dynamics. However, they did not study the interplay of topography and geological heterogeneity. Few studies conducted on tile drain flow modeling emphasized the importance of shallow geology up to 20 m depth (De Schepper et al., 2017; Hansen et al., 2019b; Hansen et al., 2019a). Mahmood et al. (2023) studied the correlation of topographical and geological variables on spatial tile drain flows. They found topographical variables such as the Topographical Position Index (TPI) and TWI to be important variables. However, the original resolution of the geological variables (100 m or 30 m) used in their study was much coarser than the topographical variables (10 m). Therefore, no significant correlation was found between geological variables and spatial tile drain flow. Past studies provide an understanding of the geological influence on the tile drain flow at field scale. However, the interaction of topographical and geological variables that control the spatial pattern in tile flow generation via distinct flow paths is still not fully understood or quantified.

In Denmark, most agricultural land is tile drained with clayey till geology, however, among the clayey till geology heterogeneity still exists, e.g., high hydraulic conductivity lenses are present in the otherwise lower hydraulic conductivity clayey till (Kessler et al., 2012). These sand lenses are of great importance for flow pathways (Nilsson et al., 2001). Thus, their representation in models is crucial to predict tile drain flows accurately. Different approaches have been used in the past for representation and translation of geological heterogeneity into hydrological models (Boico et al., 2022; De Schepper et al., 2017; Hansen et al., 2019b). However, none of these approaches focused on the representation of geological heterogeneity in the upper 5 m of the geological layers and its impact on the spatial variation of tile drain flows. Therefore, this study focused on the detailed representation of geological heterogeneity in hydrological models for shallow depths (0–5 m) that we hypothesize is the key to understand tile drain flows. Apart from studying the impact of heterogeneity on spatial distribution of tile drain flows, the novelty of our work included the use of a new approach in mapping and modeling of shallow geology using multiple geophysical instruments. First, the unique approach applied in this study combined geophysical data from two different geophysical instruments to obtain detailed in-depth 3D geophysical voxel model for the study area using a geostatistical method called Multi point statistics (MPS). Second, the 3D geophysical voxel model together with the hydraulic conductivity estimates were used to develop geological models that were fed into groundwater models. We also investigated the interplay between geology and topography on the spatial distribution of the tile drain flow, which has not been explored in detail in previous studies.

The objectives of this study were: 1) to investigate the combined effect of topographical characteristics and geological heterogeneity on the spatial pattern of the tile drain flows; and 2) to assess the effect of high hydraulic conductivity lenses on the spatial pattern of the tile drain flows. To achieve these objectives, we developed high resolution 3D geological models using high resolution geophysical data, and hydraulic conductivity measurements using slug tests at multiple locations and depths. Furthermore, to assess spatial patterns of the tile drain flow for different geological models, we optimized three groundwater flow model scenarios to simulate tile drain flows. Lastly, we explored the relation of spatial patterns of tile drain flow of three different geological models with TI.

2. Site description

The study site is located in a moraine landscape 20 km south of the city of Aarhus, Eastern Jutland, Denmark (55°59′N 10°4′ E,

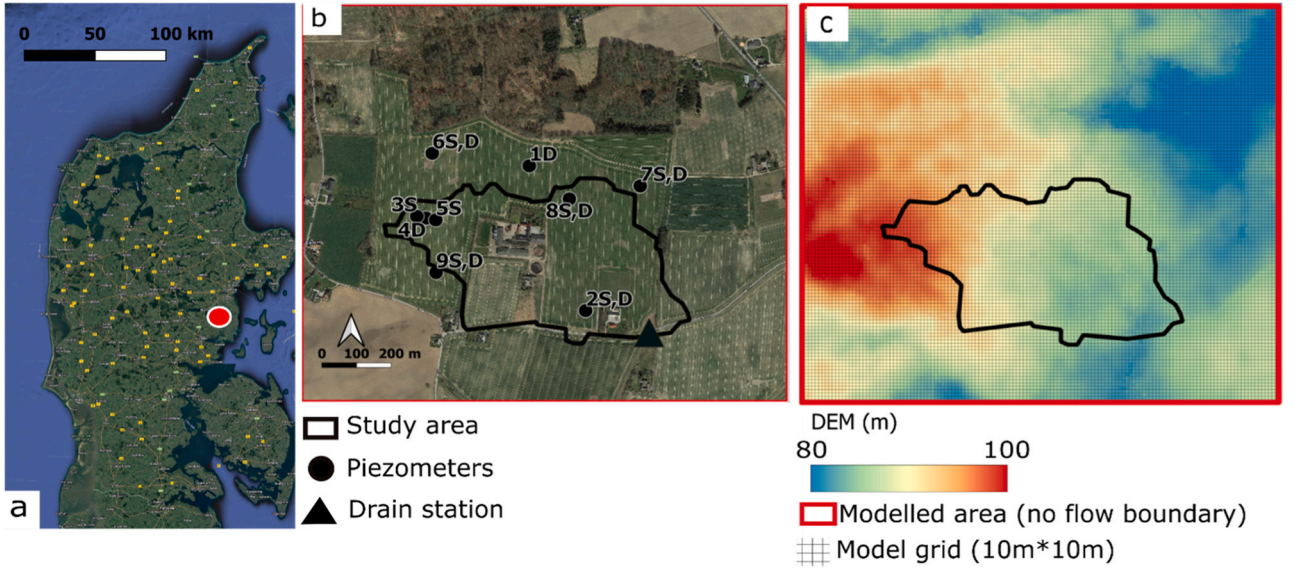

Fig. 1. The location of the study site in Denmark (a) and the location of piezometers and tile drain outlet in the study site (b) conceptual model with the modelled area, digital elevation model and model grid (c). In Fig. 1b, the suffix D in the piezometer ID indicates deep piezometer with depth till 5 m and screen depth of 2–5 m while suffix S in piezometer ID indicates shallow piezometer with depth of 1.5 m screen depth of 0.4–1.5 m. The recharge and drain package are applied to full model grid.

Fig. 1a). The site lies within the larger Fensholt catchment (6 km^2) covering an area of 28 ha (Fig. 1b). Approximately 87 % of the site area is used for tillage and is systematically tile drained. The topography is gently undulating, and the land surface elevation ranges from around 82 m above sea level in the southeast to 98 m in the northwest. The geology consists of a 15–30 m thick cover of Quaternary glacial deposits composed of clayey and sandy sediments. The predominant soils in the study area are morainic clays (De Schepper et al., 2017) and the soil texture is primarily sandy loams (Varvaris et al., 2018). The climate is characterized by mild winters, cool summers, and frequent precipitation, with an annual precipitation of 870 mm/yr (unpublished data for 2012–2017). The average groundwater recharge is estimated to be 420 mm/yr (unpublished data for 2012–2017). The recharge data was calculated previously from the EVACROP model (Olesen and Heidmann, 2002) where evapotranspiration is subtracted from the precipitation (simulated daily recharge is given in Fig. 6). The agricultural area is completely rain-fed so no irrigation methods are used in this study area. There were 14 piezometers installed in the study area (black dots in Fig. 1b): 7 deep piezometers and 7 shallow piezometers. The deep piezometers were screened between 2 and 5 m while the shallow piezometers were screened between 0.4 and 1.5 m. Tile drain flow from the whole study area was collected at the drain station (see location in Fig. 1b) using flow meter at sub-daily intervals. The data was obtained as pulses (1 pulse =100 litres), which were summed for the whole day and tile drain flow of the whole study area was calculated.

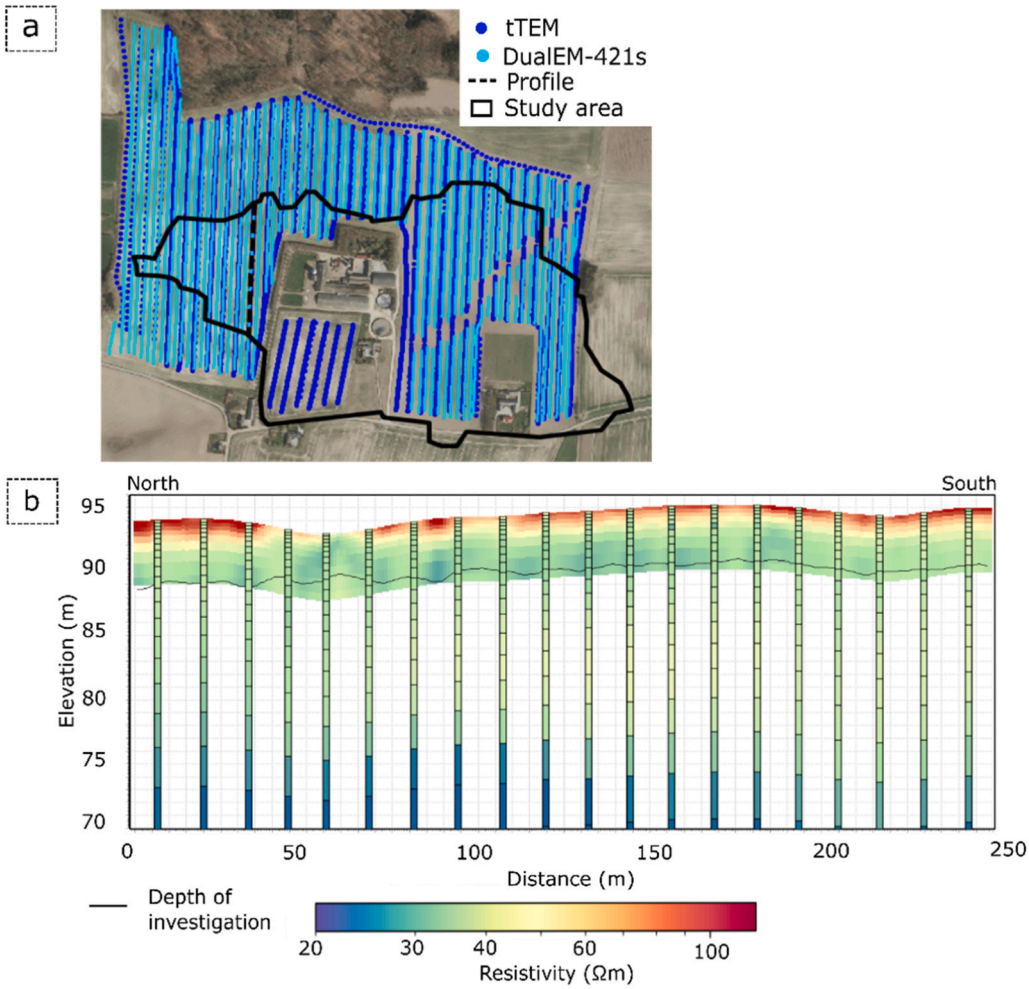

Fig. 2. Geophysical sounding position (a) and cross-sectional view (b). The light blue color indicates DualEM-421 s sounding positions, and the dark blue color indicates tTEM soundings (a). The cross-sectional view of dense DualEM-421 s′ recovered resistivities are from 94 m to 88 m elevation. Electrical resistivity from 94 m to 70 m indicates tTEM recovered resistivities (b). In Fig. 2b, the left side indicates north of the cross-section and right side indicates south of the cross-section. The black line in the cross-section indicates the depth of reliable DualEM-421 s recovered resistivities.

3. Materials and methods

3.1. Mapping and modeling of geology

3.1.1. Geophysical mapping and recovered resistivities

The site was intensely mapped with two surface geophysical methods: a Frequency-domain Ground conductivity meter system (DUALEM-421s) for the shallow subsurface (0–5 m depth) (McNeill, 1980) and a Time-domain towed-transient electromagnetic method (tTEM) for the deeper geology (5–80 m depth) (Auken et al., 2018a). The datasets for the DUALEM-421s and tTEM were both collected using an ATV providing continuous data, which were later processed to individual soundings at certain intervals. The two data sets were processed and inverted independently. The data were inverted using a pseudo-3D spatially constrained inversion (Viezzoli et al., 2009) setup based on a 1D forward algorithm with a sharp model formulation (Vignoli et al., 2015). This setup was recommended by Christiansen et al. (2016) and Frederiksen et al. (2017). The DualEM-421s instrument collects data at 9000 Hz at 3 different coil-separations giving 6 data points per sounding in total (DUALEM-INC, 2021). While driving the ATV along a line, the soundings were acquired for DualEM-421 s at a distance of 1 m and the spacing between two parallel lines was kept around 11 m (Fig. 2a). A total of 25,407 DUALEM-421 s soundings were collected. The tTEM instrument is a time-domain electromagnetic instrument where a transmitter coil and a receiver coil are pulled by an ATV (Auken et al., 2018b). The tTEM data were collected using two magnetic moments giving a total of about 25–30 data points, depending on the signal to noise level. While driving the ATV along a line, the recovered resistivities of the tTEM soundings were acquired at 10–13 m, and the distance between the lines was about 22 m (Fig. 2a). The total number of tTEM soundings were 2151.

3.1.2. Gap filling and development of a 3d geophysics voxel model

Recovered resistivities of the DualEM-421s and tTEM were obtained in the form of 1D models at each sounding position. The sounding positions are spaced differently for tTEM and DUALEM-421 s (explained in Section 3.1.1), and the 1D models had a different depth discretization. Moreover, parts of the site were not mapped due to fences and pavement, constituting 13 % of the site (Fig. 2a). In order to prepare the geophysical model to inform the hydrological model, we needed to build a complete 3D model. Therefore, the gaps in coverage of the recovered resistivities were filled in two steps. First, the recovered resistivities were interpolated to a uniform 3D grid by S-GeMS, (Remy, 2005) using kriging, which was discretized into 10 by 10 by 1 m voxels (x, y, z, respectively) to cover the same volume as the groundwater model (see Section 3.2). As indicated in Section 3.1.1, we used model information from DUALEM-421 s for the first 5 m and information from tTEM for 5–80 m depth. Second, the gaps in the 3D voxel model were filled using the known complex geological patterns of the area by the MPS algorithm 'Direct Sampling' (Daly and Caers, 2010; Mariethoz et al., 2010). We used MPS because it captures complex geological patterns using training images from the study area that other interpolation methods such as kriging and inverse distance weighting cannot capture to the same degree. This characteristic is specifically important to capture heterogeneity in the geological models (Atkinson and Lloyd, 2010). We chose the MPS method - direct sampling because it is fast and easy to use, but many other MPS algorithms could have been used equally well. The total depth (z) of the voxel model was 80 m and it was later used as the skeleton of the different geological models.

3.1.3. Hydraulic conductivity estimation

The purpose of estimating hydraulic conductivity at different electrical resistivities was to quantify the ranges of hydraulic conductivity values that can be found in the area. The hydraulic conductivity up to 0–5 m soil depth was estimated using slug tests (Cheremisinoff, 1998) in areas with low and high electrical resistivities. A slug test refers to restoring the hydraulic head to its equilibrium state after introducing a sudden change in the hydraulic head of a well. In the current study, this abrupt change was caused by removing water from the well. The recovery of water heads towards the equilibrium head level was measured as a function of time. We used the Hvorslev method to estimate the hydraulic conductivity (Cheremisinoff, 1998; Schwartz and Zhang, 2003).

In Eq. 1, the drawdown ratio is used, which is the ratio of drawdown s_t at any time 't' to the initial drawdown 's_0' when the test starts at 't_0' ($H_t = s_t/s_0$). The drawdown ratio is plotted with time on a semi-log scale (where drawdown ratios are plotted on a logscale, and time is plotted on a normal scale). A straight-line is fit in order to find the slope, which is required to calculate K from the equation (Cheremisinoff, 1998; Schwartz and Zhang, 2003).

$$K = \frac{R^2}{2L(t_2 - t_1)}.\ln\left(\frac{L}{R}\right).\ln\left(\frac{H_1}{H_2}\right) \quad for \frac{L}{R} > 8 \tag{1}$$

Where, L is the length of screen, R is radius of piezometer, t_1 and t_2 are time and H_1 and H_2 represent the drawdown ratios at time t_1 and t_2.

The slug test was performed in 7 piezometers with a screen depth of 0.4–1.5 m (with suffix 'S' in Figs. 1b) and 7 piezometers with a screen depth of 2–5 m (with suffix 'D' in Fig. 1b). The pressure transducers were installed in the piezometers to collect data in 10 min interval for the slug test. The recovery of the water level was recorded as a function of time using data loggers every 10 min. These hydraulic conductivity estimates were used to determine the average low and average high hydraulic conductivity of the Fensholt-D3 drain site. The slug test experiment was repeated 3–5 times for each piezometer to obtain statistically sound hydraulic conductivities.

3.1.4. Translation of electrical resistivities into hydraulic conductivity

For the development of the geological models, we assumed that soil properties can be interpreted from electrical resistivity

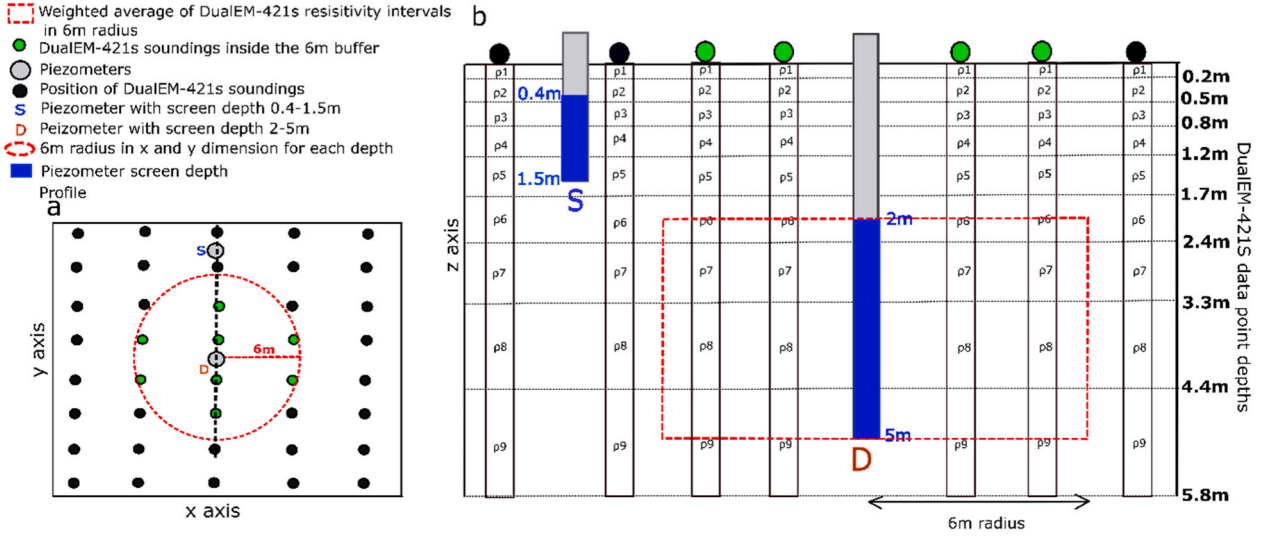

Fig. 3. Schematics showing example of DualEM-421 s sounding depth intervals and piezometer's screen depths. The aerial view of the dualEM-421 s and piezometer is given in (a). The cross-sectional view of the dualEM-421 s soundings with its resistivity intervals and piezometer screen depths is given in (b).

measurements. Hansen et al. (2019b) and Boico et al. (2022) also used this approach to delineate high and low hydraulic conductivity zones. Therefore, to convert the voxel model into different geological models and to determine hydraulic conductivities of the geological models, we compared the hydraulic conductivity estimates from the piezometers (0–5 m of soil) with its corresponding electrical resistivity data (Fig. 4). Moreover, the link between electrical resistivity, geology, and hydraulic conductivity was supported by borehole sediment logs of the study area. Two aspects had to be addressed for this comparison. First, the recovered resistivities obtained from the DualEM-421 s were more accurate and denser than the recovered resistivities of the tTEM for 0–5 m depth. Therefore, we only used DualEM-421 s measurements for the comparison of hydraulic conductivities and electrical resistivities. The recovered resistivities from the tTEM and the geophysics voxel model, were not used for this comparison. Second, the depth discretization of the DualEM-421 s and the hydraulic conductivities were not directly comparable. The recovered resistivities of the DualEM-421 s were distributed in a 3-dimensional space with a non-uniform depth spacing (see Fig. 3b). The hydraulic conductivity estimates at screen depths of 0.4–1.5 m for S piezometers and 2–5 m for D piezometers were not directly comparable to the depths of the DualEM-421 s (see Fig. 3b). To address this concern, we first calculated the geometric mean of electrical resistivities using a 6 m radius (x and y dimension, see Fig. 3a) at each depth interval of the DualEM-421 s. Then, a weighted average of electrical resistivity of the DualEM-421 s was taken by the fraction of depth (z dimension) corresponding to screen depths of the piezometers. The 6 m radius was selected to ensure that there were at least three neighboring DualEM-421 s electrical resistivity points for each piezometer.

3.1.5. Geological model scenarios

After comparing the hydraulic conductivity with its corresponding electrical resistivity, we determined two hydraulic conductivity groups for both high and low electrical resistivity areas. As the aim of the study was to assess spatial patterns of tile flow generation in different geological and topographical characteristics, three different geological models were tested:

Simulation 1: 'Uniform Low K': geological model with homogeneous low hydraulic conductivity.

Simulation 2: 'Uniform High K': geological model with homogeneous high hydraulic conductivity.

Simulation 3: 'Distributed K': geological model with high hydraulic conductivity lenses. For the distributed K, the voxel geophysics model was utilized to separate high and low resistivity areas using a specific electrical resistivity threshold. High hydraulic conductivity was assigned to high resistivity areas (areas with electrical resistivity above threshold value), and low hydraulic conductivity was assigned to low hydraulic conductivity areas (areas with electrical resistivity below threshold value).

The relation of the mapped electrical resistivity with the estimated hydraulic conductivity for the 14 piezometers helped to establish a group with low hydraulic conductivity values and a group with high hydraulic conductivity values. Both groups are shown in Table 1 and Fig. 4. The three geological models served as the baseline for three distinct hydrological model scenarios.

3.2. Groundwater model setup and evaluation

3.2.1. Model design

A transient groundwater model was constructed using MODFLOW 6 (Langevin et al., 2017). The simulation period was from 01-Apr-2013–31-Mar-2016, where the first year was used as a warmup period, the second year was used as a calibration period, and the third year was used as a validation period. The three-dimensional model applied a uniform horizontal nodal spacing of 10 m with 120 rows (north to south) and 140 columns (east to west). Topography is included in the model discretization package. The model area was kept larger than the actual study area to allow lateral flows in and out of the site. No flow boundary was applied at the outline of the modelled area shown in Fig. 1c. Drainage and recharge was represented in the whole model grid as a head dependent flux boundary. Water entered the groundwater system as a uniform recharge to the water table (whole model grid). As recharge was calculated for the study area using the EVACROP model, therefore, the unsaturated flows were not simulated in the groundwater model. The model was simulated as an isotropic and an unconfined aquifer. The model had six layers: the upper five layers were 1 m

Table 1
List of the electrical resistivity estimates from DualEM-421 s and the hydraulic conductivity estimates from the slug test for the 14 piezometer locations.

Piezo ID	Screen depth (m)	Mean electrical resistivity (Ωm)	Mean hydraulic conductivity (m/d)	No. of slug test	Group division using 50 Ωm threshold	Average hydraulic conductivity of groups (m/d)
1d	2–5	32.9	2.96E-03	6	Group 1 (Low hydraulic conductivity)	0.003
2d	2–5	29.9	3.72E-03	4		
3d	2–5	33.4	3.78E-03	6		
4d	2–5	35.2	5.50E-04	5		
5d	2–5	34.9	3.85E-03	7		
6d	2–5	35.7	1.26E-03	6		
7d	2–5	48.9	4.54E-03	3		
1s	0.4–1.5	31.6	6.05E-03	7		
2s	0.4–1.5	44.7	1.70E-03	5		
3s	0.4–1.5	35.5	1.93E-03	6		
4s	0.4–1.5	43.3	1.95E-02	6		
5s	0.4–1.5	96.5	4.33E-02	5	Group 2 (High hydraulic conductivity)	0.21
6s	0.4–1.5	87.1	3.54E-01	3		
7s	0.4–1.5	72.9	6.32E-01	5		

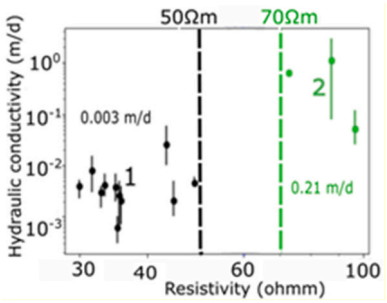

Fig. 4. Scatterplot of electrical resistivity vs hydraulic conductivity.

thick, while the bottom layer was 15 m thick. Based on our analysis (can be verified from Fig. 2b, Fig. 5b) and past studies in the study area (De Schepper et al., 2017; Hansen et al., 2019a), the study area has a thick clay layer below 15–20 m depth, so layers below 20 m depth were not included in the model.

MODFLOW 6 has a drainage (DRN) package to simulate the effects of agricultural drains. The DRN package in MODFLOW6 is based on the principle of a head-dependent flux boundary rather than representing actual drainpipes. With this boundary condition, if the groundwater head (h) in the cell falls below the drain depth (H_{DRN}), the flux (Q) from the model cell to the drain drops to zero. If h in

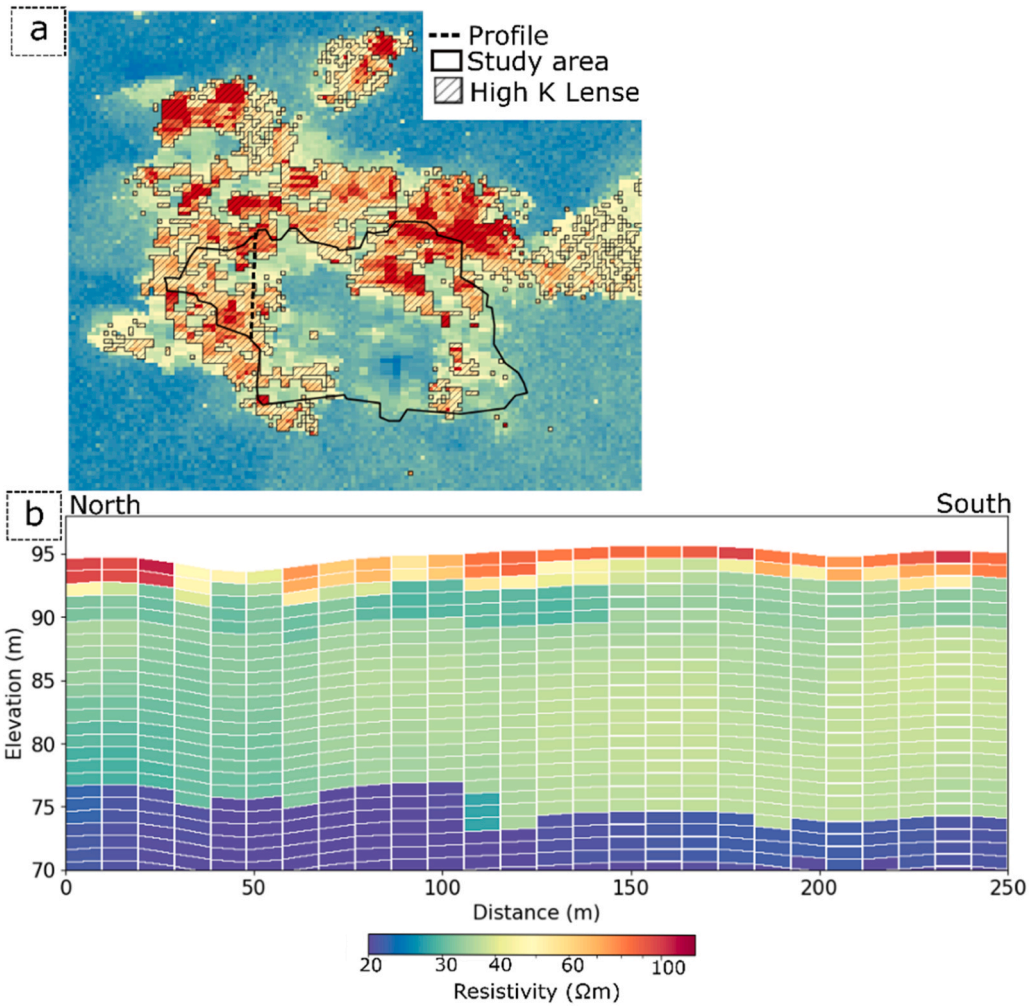

Fig. 5. Geophysics voxel model aerial and cross-sectional view. The aerial view of the top layer of the geophysics voxel model with delineation of high hydraulic conductivity lenses (a). Fig. 5b indicates the cross-sectional view of the black dashed line in (5a). In Fig. 5b, the left side indicates the north of the cross-section and right side indicates the south of the cross-section.

the cell rises above H_{DRN}, Q is linearly dependent on a specified drain conductance (C_{DRN}) and the difference between the head (h) and H_{DRN} (Langevin et al., 2017) is calculated as:Langevin et al. (2017).

$$Q = C_{DRN}(h - H_{DRN}) \tag{2}$$

The depth, spacing, and location of drains were unknown in the study area. The drains were represented in all nodes around 10 m apart in model layer 1 at 0.9 m depth with the assumption that all fields that need to be drained have active drains. The exact location of tile drains is important to include in the model, however, we knew that in our catchment tile drains were everywhere. Therefore, we believe it was a valid assumption that all areas that should be drained are drained. The drains were only activated when the water level was above draining depth at a particular time. Schilling et al. (2019) and Mahmood et al. (2023) have also used similar approach for studying tile drain flows. As the drain depth (H_{DRN}) and drain conductance (C_{DRN}) were also unknown in the study area, a H_{DRN} value (0.9 m) and a C_{DRN} value (10 m2/day) were taken from literature (Hansen et al., 2013; Hansen et al., 2019a). In the model, water which is drained from a grid cell is considered to exit the model and cannot re-infiltrate in the model grid cell downstream.

3.2.2. Model calibration

The model was calibrated for a specific yield (Sy) and a specific storage (Ss) using the Parallel Pareto archived dynamically dimensioned search (ParaPADDS) algorithm (Asadzadeh and Tolson, 2013; Matott, 2017) in OSTRICH tool (Matott, 2017). OSTRICH is a model-independent optimization tool that includes different multi-objective optimization algorithms and ParaPADDS is one of the many algorithms used for multi-objective function optimization (Asadzadeh and Tolson, 2013; Matott, 2017). ParaPADDS determines a Pareto-front, which enables the evaluation of trade-offs between multiple objective function groups without the need to assign weights to these groups before calibration. For our calibration, we utilized two objective function groups: Kling-Gupta efficiency (KGE) and percentage bias (PBIAS), between the daily simulated and observed tile drain flow at the outlet. KGE and PBIAS were included in the objective function because they serve different purposes. KGE is used to evaluate the temporal dynamics of the tile drain flow, while PBIAS is used to determine whether the model over-estimates or under-estimates the simulated tile drain flows. The Sy and Ss parameters were optimized as calibration parameters. All three groundwater model scenarios; Uniform low K, uniform high K and distributed K, were calibrated separately. After calibration, the model scenarios were run for a validation period from 01-April-2015–31-Mar-2016.

3.3. Data analysis

To assess the effect of topography and geology on the tile flow generation we (1) computed the drainage fraction (DF) and two topographical indices (TI) in a 10 m x 10 m resolution for the study, and (2) calculated the Pearson correlation between the DF and the two TIs.

The DF was calculated for each model scenario to analyze differences in tile drain flows in different geological models. The DF is the ratio between tile drain flow and recharge. It was calculated for the simulation period for each cell for the top layer (layer 1) in the models, as it is the layer where recharge takes place and where the drains are located. The DF is calculated as

$$DF = \frac{\sum_{t=1}^{N} d}{\sum_{t=1}^{N} r} \tag{3}$$

In Eq. 2, d is the tile drain flow volume at a specific cell, r is the groundwater recharge volume at a specific cell, t is the stress period (day), and N is the total number of stress periods (365 days). The DF becomes zero when there is no discharge to recharge, and it becomes one when all recharge is the same as drains. The DF can be above 1 due to lateral fluxes from neighboring cells or upward fluxes from deeper layers. The DF was calculated for each model scenario to analyze differences in tile drain flows in different geological models.

The two topographical indices, the Topographical Position Index (TPI) and the Topographical Wetness Index (TWI), were computed using the digital elevation model. The TPI relates the elevation of a pixel to the average elevation of the neighboring pixels within a certain radius (70 m in this study) (Gallant and Wilson, 2000). A negative TPI value indicates local valleys, and a positive TPI value indicates local hills.

TWI relates the upslope contribution area with the slope (Mattivi et al., 2019) and is calculated as:

$$TWI = \ln\left(\frac{x}{\tan(y)}\right) \tag{4}$$

where x is the upslope contributing area and y is the slope in radians. A high TWI indicates that more water accumulates in that cell.

4. Results and discussion

4.1. Mapping and modelling of geology

The electrical resistivity models of the tTEM and DualEM-421 s are shown in Fig. 2b. The electrical resistivities ranged from 20 Ωm to 120 Ωm. Relatively high electrical resistivity above 50 Ωm was observed in 0–3 m of the soil, while lower electrical resistivities were observed with depth. The tTEM model below 20 m depth showed the lowest resistivity value of 20 Ωm in the study area (in Fig. 2 below

75 m elevation). The low electrical resistivity around 20 Ωm indicated the presence of a thick clay layer (aquitard). It is also clear that the recovered resistivities of the DualEM-421 s detected a detailed variation in electrical resistivity up to 5 m depth, which could not be distinguished in the tTEMs' recovered resistivities (see Fig. 2b).

The results of the 3d geophysics voxel model are shown in Fig. 5. Fig. 5a shows the aerial view of the first layer of the voxel model. The geophysical data gaps in the central and southern part of the study area were filled in the voxel model. The north and north-

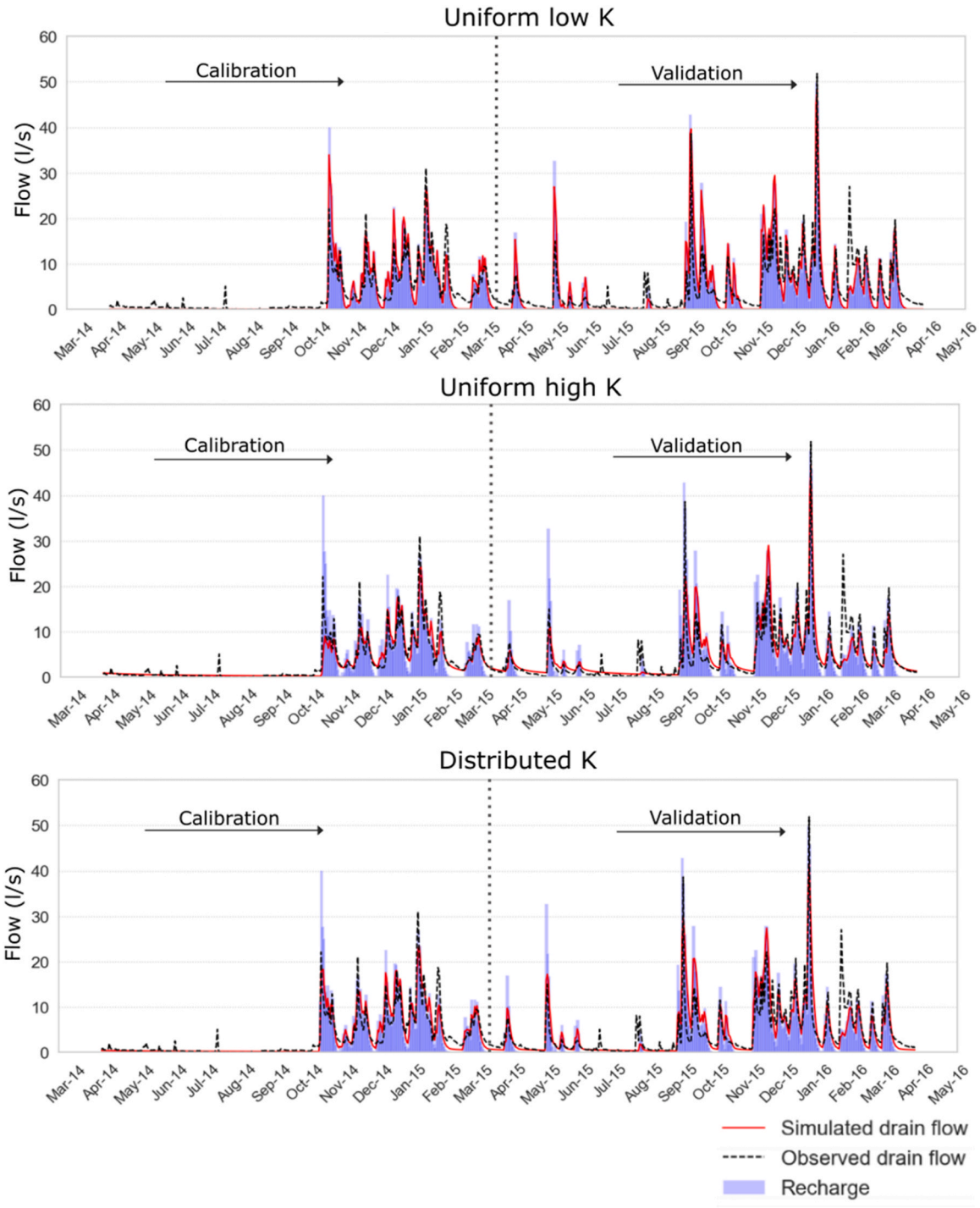

Fig. 6. Hydrographs of the daily simulated tile drain flow, the observed tile drain flow and the observed recharge for model simulations, Uniform low K, Uniform high K, Distributed K. All three model scenarios were successful in predicting the tile drain flow dynamics and volumes of the study area. Despite the good model performance, the model scenarios produced different DF values.

western part of the study area depicted a high electrical resistivity while the central and southern part of the study area showed a low electrical resistivity (Fig. 5a). Like the recovered resistivity results (Fig. 2), the cross-sectional view of the 3d geophysics voxel model also showed high electrical resistivities of above 50 Ωm at 0–3 m depth and low electrical resistivity below 50 Ωm below 3 m. The electrical resistivity was the lowest in the study area below 20 m depth (at 75 m elevation, Fig. 5b).

The comparison between hydraulic conductivity estimates from slug tests and electrical resistivity measurements from the DUALEM-421 s showed a trend of high hydraulic conductivity values in high resistivity areas and low hydraulic conductivity values in low resistivity areas. The hydraulic conductivities were between 10^{-4} and 10^{1} m/d, with most values around 10^{-3} m/d (Table 1), which fits adequately with the clayey till in the area.

Two groups were established, one with low hydraulic conductivity values (0.003 m/d, group 1) and a group with high hydraulic conductivity values (0.21 m/d, group 2). Both groups are shown in Table 1.

For the delineation of the high hydraulic conductivity lenses in the area, the threshold of 50 Ωm electrical resistivity was arbitrarily selected. There were no hydraulic conductivity estimates between the 50 Ωm to 70 Ωm electrical resistivities (shown in Table 1) and the main aim of the study was to assess the influence of geological heterogeneity and topography on the DF. Therefore, we believed selecting any threshold between a 50 or 70 Ωm electrical resistivity would support the aim of the study.

4.2. Groundwater model performance

The three models matched the observed daily tile flow with a few offsets in the magnitude of the peaks (Fig. 6 and Table 2). The optimized parameters for the three models were slightly different, but within acceptable ranges, except for the Sy value of uniform high K (Table 2). The Sy value is lower than what is expected for a high hydraulic conductivity scenario, however, it is consistent with the characteristics of the study area – being clay dominant with a small proportion of high hydraulic conductivity lenses. In the distributed K, the Sy_{max} value was closer to reality for the high hydraulic conductivity zone as suggested in Heath (1983) and Johnson (1967). All three model scenarios depicted a similar trend in the timing of the tile drain flow (KGE values from 0.73 to 0.90) and the volumes (PBIAS values from –3.39 to 0.94) between the simulated and the observed tile drain flow. KGE and PBIAS were both best optimized for distributed K. PBIAS was negative (that is, on average the simulated tile drain flow is less than the observed tile drain flow) for uniform high K and positive for distributed K and uniform low K. However, all model scenarios were able to predict the tile drain flow dynamics.

In the validation period, all model scenarios were still within an acceptable range. The timings of the tile drain flow (KGE values from 0.66 to 0.84) and volumes (PBIAS values from 4.75 to 6.95) showed similarities between the simulated and the observed tile drain flow. However, the PBIAS indicated an overestimation in volumes for all model scenarios.

4.3. Spatial patterns in tile flow generation

The model scenarios had similar spatial patterns of DF in uniform high K and uniform low K (Fig. 7). However, the introduction of high hydraulic conductivity lenses in the distributed K scenario significantly changed the DF distribution as it showed a combination of DF from uniform low K and uniform high K. On a local scale, the models had a higher DF in topographical depressions and a lower DF in topographical highs.

The model scenarios, however, had different ranges of DF (Fig. 7, Table 3). The uniform low K model scenario had the smallest 5–95 % percentile range in the DF: from 0.90 in topographical highs to 1.10 in topographical depressions (Table 3). The uniform high K model scenario, on the other hand, had the largest 5–95 % percentile range in the DF: from 0 to 3.60 (Table 3). The distributed K model scenario has an intermediate 5–95 % percentile range in the DF: from 0.32 to 1.73, in between the two uniform K model scenarios - uniform low K and uniform high K (Table 3).

In addition to the spatial variability in the DF, we looked at the differences in the transience in the discharge between the three scenarios. That is, the regularity of discharge changes from the average state. The strength of the discharge was relatively constant over time in the uniform low K model scenario, as evidenced by the smallest 5–95 % percentile range in the coefficient of variance (CV) (1.67 in topographical depressions and 1.87 in topographical highs, Table 3). Contrary to this, the uniform high K model scenario does not have this strong, consistent flow and is more easily affected by changes in the groundwater stage, as is shown by the larger 5–95 % percentile range in CV (1.05–12.45, Table 3). The distributed K model scenario is intermediate between the two uniform K model scenarios (Table 3). The relation of the DF to the transience in the discharge was linear, reflecting the range of stability resulting from the different degree of discharge from the groundwater flow system.

Despite the differentiated DF values between the uniform K model scenario, the spearman correlation between the spatial DF of uniform low K and uniform high K was the highest (R=0.96). This indicated a monotonic and ranked correlation between the spatial

Table 2
Parameters and performance metrics of model simulation.

Model scenario	Calibration		Validation		Parameters				
	PBIAS (%)	KGE	PBIAS (%)	KGE	K_{min} (m/day)	K_{max} (m/day)	Sy_{min}	Sy_{max}	Ss (/m)
Uniform low K	0.94	0.73	4.75	0.66	0.003		0.02		4.13E-06
Uniform high K	-3.39	0.87	6.96	0.84	0.21		0.03		4.13E-06
Distributed K	0.20	0.90	5.97	0.80	0.003	0.21	0.03	0.15	6.00E-06

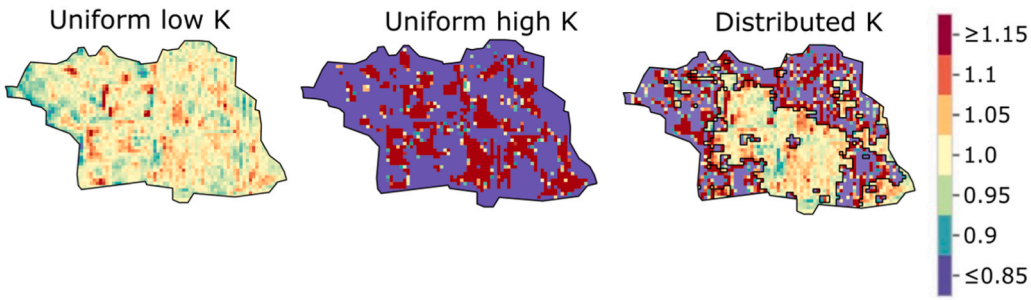

Fig. 7. Spatial patterns in DF for all three model scenarios averaged across one year. The black line shows the transitioning boundary between high hydraulic conductivity and low hydraulic conductivity.

Table 3
Statistical characteristics of spatial DF (DF) and coefficient of variation (CV).

Percentile	Uniform high K		Uniform low K		Distributed K	
	DF	CV	DF	CV	DF	CV
5-th percentile	0.00	1.05	0.90	1.67	0.32	1.07
25-th percentile	0.10	1.75	0.96	1.79	0.81	1.62
50-th percentile	0.45	2.65	0.98	1.83	0.98	1.79
75-th percentile	1.23	4.88	1.02	1.84	1.07	1.85
95-th percentile	3.60	12.45	1.10	1.87	1.73	2.79
Dominant flow system	Field (1–10 ha)		Local (10×10m)		Mix	

DF of the uniform low K and uniform high K. The areas corresponding to a high DF in high hydraulic conductivity also show a high DF in low hydraulic conductivity and vice versa. Hence, hydraulic conductivity changes the magnitude and range of DF values.

4.4. Effect of topography and geology on tile flow generation

The TWI values ranged from 11 to 18 in the study area, with most values between 13 and 15 (Fig. 8). High values formed a stream-like network, which indicated the influence of the upslope contributing areas stretching from northwest to southeast (Fig. 8). The values of the TPI were between –0.75–0.75 (Fig. 8).

The DF was related to the TPI (R values from –0.87 to –0.52 in Fig. 9b), which suggested that the DF is controlled by small-scale topography, whereas, the DF was weakly correlated to the TWI (R values from 0.37 to 0.21 in Fig. 9a). Thus, the TPI is more appropriate than the TWI for assessing spatial variability of the DF in clayey moraine landscapes.

The relationship between the DF and the TPI was stronger for the uniform K models (R = –0.77 and R= –0.87) than for the distributed models (R= –0.52). The slopes among the uniform K model scenarios were significantly different; the uniform low K model scenario had a lower slope (–12.66) than the uniform high K (–283.34); higher hydraulic conductivity increased the effect of local topographic depressions and peaks on DF. The heterogeneous model scenario depicted combinations of two correlation systems: a steep slope for high hydraulic conductivity lenses and a flat slope for low hydraulic conductivity areas (Fig. 9).

Motarjemi et al. (2021) found an ambiguous correlation between the average tile drain flows and the topographic elevation at field scale. They observed a high tile drainage flow both in elevations above 40 m and below 30 m. The reason they were not able to find a clear correlation is that topographic elevation itself does not affect the tile drain flow; it is instead the localized relative differences in

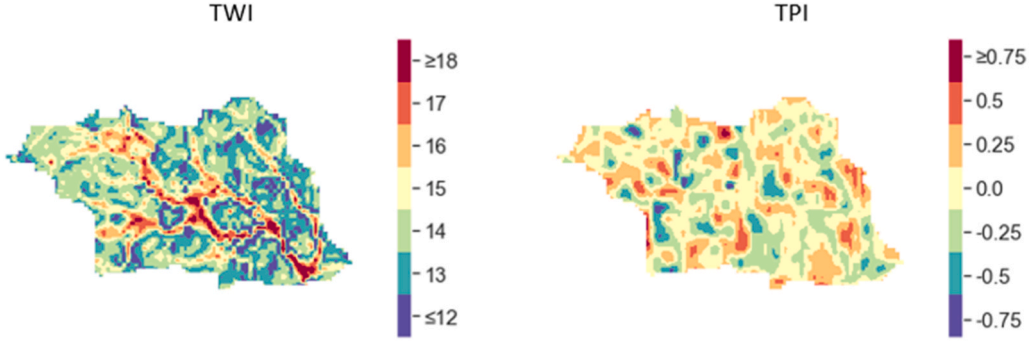

Fig. 8. TWI and TPI for the model area.

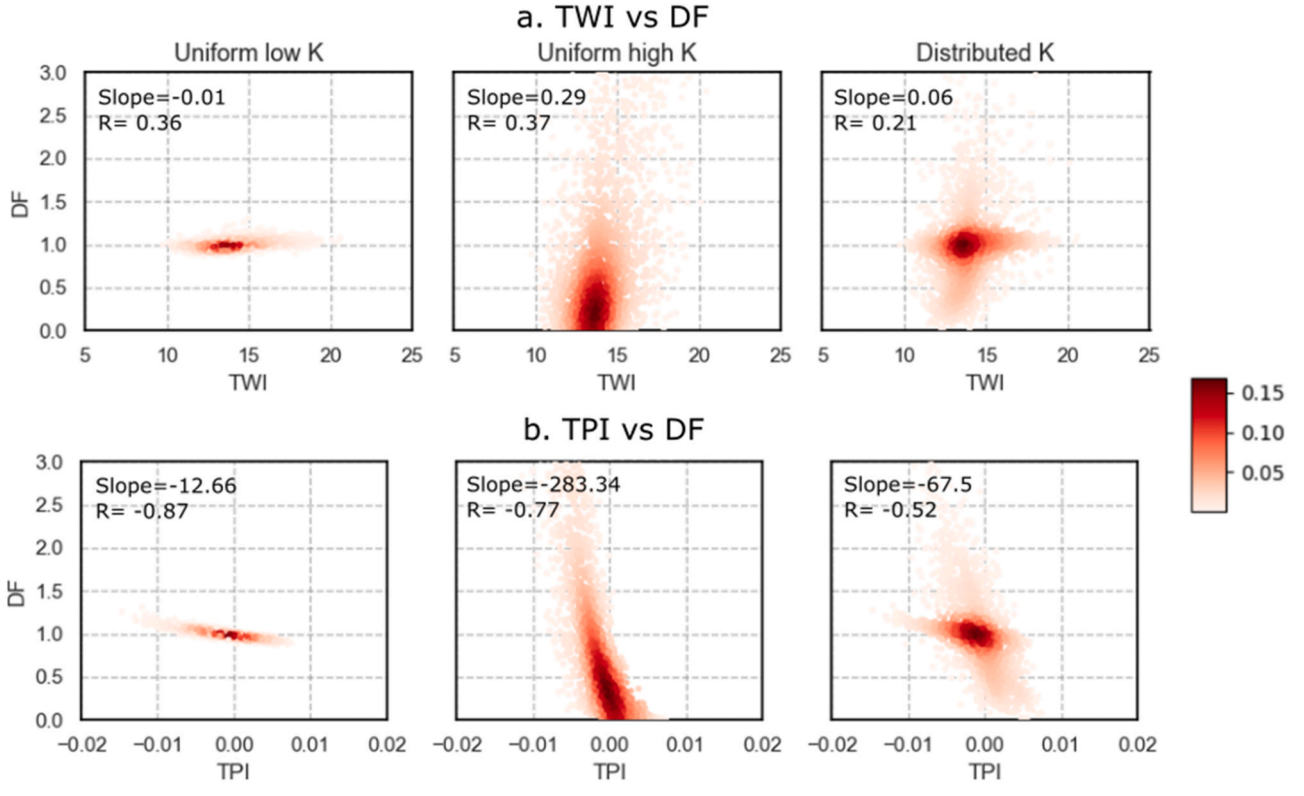

Fig. 9. Linear models that relate discharge fractions to TWI and TPI, respectively. The color bar represents the density of data.

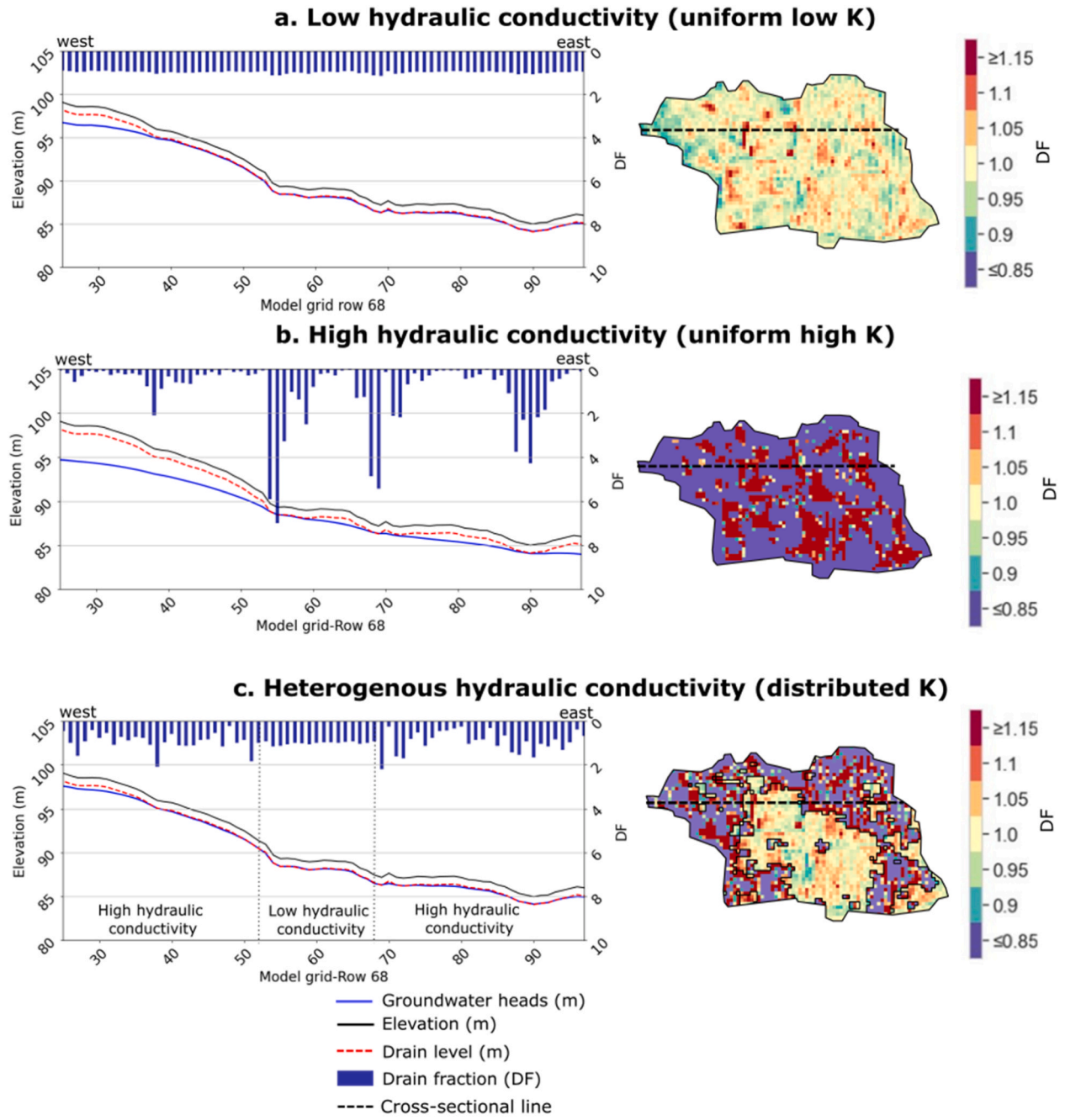

Fig. 10. Interplay of geology and topography. Example of hydrological flow using a cross-section of a. Uniform low K (low hydraulic conductivity); b. Uniform high K; c. Distributed K (heterogeneous hydraulic conductivity). The DF and groundwater heads are averaged across a year.

topography that regulate the tile drain flow. We also found that the DF was weakly correlated to the TWI on the localized scale of 10 × 10 m (R values from 0.37 to 0.21 in Fig. 9a), which is consistent with the past results obtained by Hansen et al. (2019a) at large scale 100 × 100 m. This was because the TWI highlights connected regions and their potential water flow paths. The influence of elevation (above mean sea level) is more dominant in the TWI. On the other hand, the TPI shows a localized scale variability independent of the elevation above sea level. In regions where detailed groundwater models cannot be developed or where limited information about geology and geological heterogeneity is known, this correlation analysis between TPI and DF could be beneficial for water managers to understand the spatial tile drain flows and drainage to recharge ratios.

Mahmood et al. (2023) studied the correlation of topographical and geological variables with spatial patterns of tile drain flows and examined the relationship between spatial patterns of tile drain flows and topographical and geological variables. Their findings revealed a significant correlation between spatial tile drain flows and topographical variables, including TPI and TWI. However, the

geological variables identified in the study, such as clay fraction and clay thickness, were not available at a high resolution comparable to the topographical variables. Furthermore, the study did not incorporate highly detailed geophysics data. Consequently, the importance of geological variables in explaining the spatial patterns of tile drain flows may have been underestimated due to the lack of adequate data resolution.

4.5. Use of geological mapping and modelling in hydrological models

Hydrological modeling requires assumptions about the subsurface structure, which can impact the accuracy of simulated hydrological processes (Voss, 2011). Introducing heterogeneity in tile drain flow modelling is crucial to map the flow patterns of the region. Though the non-invasive geophysical mapping was a rough estimate for geology, they were a better alternative to invasive methods such as localized borehole log information due to the lower cost and higher mapping resolution of the local geology. The use of two geophysics methods; DualEM-421 s and tTEM allowed to get near surface (0–5 m) and deeper electrical resistivities up to 80 m depth for the study area. Moreover, the application of MPS to fill data gaps resulting in a high-resolution 3D voxel model enabled us to delineate geological lenses with high hydraulic conductivity in high detail.

In this study we estimated hydraulic conductivity values for different parts of the study area. We believe it is crucial to estimate hydraulic conductivity values at different electrical resistivities in the study area for a more comprehensive understanding of the range of hydraulic conductivity values. While Boico et al. (2022) identified low hydraulic conductivity regions using soil types from borehole data in low electrical resistivity measurements, they did not estimate hydraulic conductivity values at different electrical resistivities. Hansen et al. (2019b) used electrical conductivity estimates for soil layers up to 3.5 m to represent high hydraulic conductivity zones for groundwater modeling. We developed a 3D geophysics voxel model using MPS and used hydraulic conductivity estimates from the study area to delineate hydraulic conductivity lenses.

4.6. Linking flow dynamics to topography and geology – local to field scale

Fig. 10 shows an example of hydrological flows in different hydraulic conductivity models that explain the interaction of geology and topography in the tile drain region at shallow depths. At field scale, the uniform high K scenario had a relatively low DF in the northwestern part of the area compared to the southeastern part (Fig. 10). This DF trend was attributed to an overall decreasing elevation from 98 m to 82 m in the study area from the northwest to the southeast. This showed that there is more water leaving the highest elevation point (DF value < 1) and flowing towards the depression region (DF value > 1). This can also be observed from the hydraulic heads in Fig. 11. The uniform high K had a high hydraulic conductivity and allowed water to travel a longer distance than the uniform low K model in the northwestern corner This suggests that high hydraulic conductivity gives more preferentiality to field scale

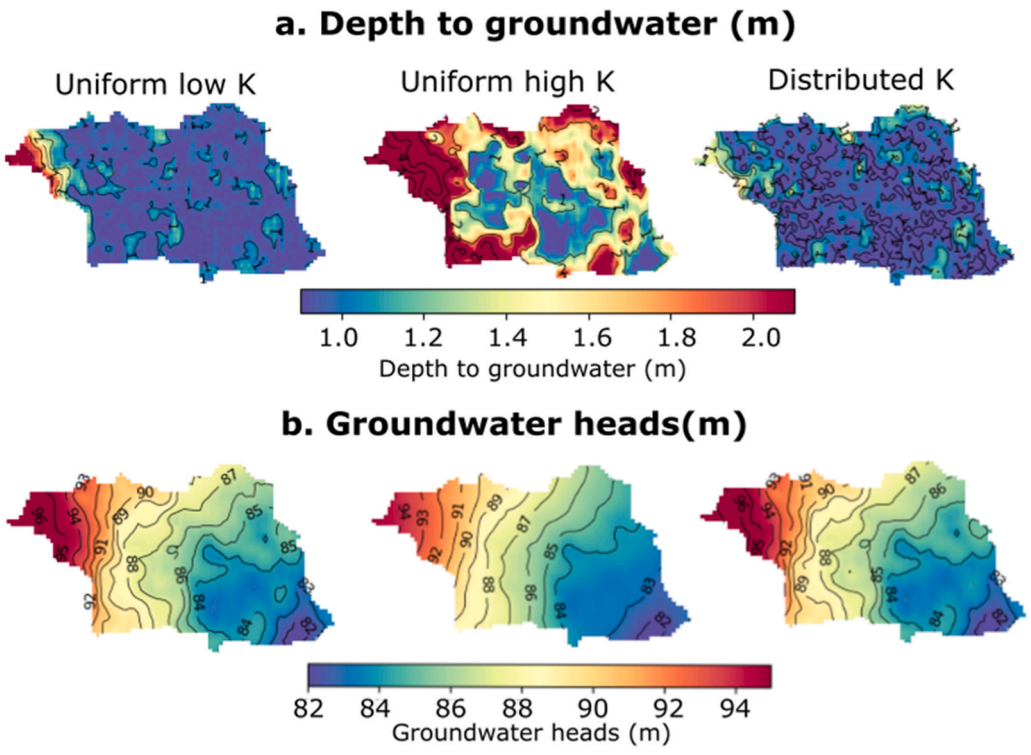

Fig. 11. Depth to groundwater heads maps for the three model simulation.

groundwater flows than low hydraulic conductivity at shallow depths. However, the drainage only affects the upper part of the groundwater system and, thus, lateral large-scale flows in lower levels could still exist.

In the high hydraulic conductivity (Uniform high K model scenario, Fig. 10), the groundwater heads were not following every local depression and hill. We rather observed a smoother decrease in groundwater heads from high topography to low topography. The DF values were mainly observed in depression regions and not in peaks. The DF values were above 1 in the depressions, which indicated that apart from recharge, field scale lateral groundwater flows were dominant. Hence, in the high hydraulic conductivity, besides recharge from precipitation, field scale lateral groundwater flows also contributed to the tile drain flow, but only in topographical depressions.

In the low hydraulic conductivity scenario (Uniform low K model, Fig. 10), the groundwater heads followed even the slightest depressions and hills of the topography. The DF in the low hydraulic conductivity was around 1, which implied that whatever was recharged is contributing to the tile drain flow. However, at every local depression, the DF was slightly above 1, and at every local hill, the DF was slightly below 1. These slight changes in the DF at the local level indicated the presence of localized flows from the nearest hills to the nearest depression. The slightly low DF in the topographical hill indicated that the recharge is slightly higher than the tile drain flow and vice versa. Hence, in case of low hydraulic conductivity, topographical depressions, and hills both contributed to the tile drain flow. Localized lateral flows were more dominant than field-scale lateral flows.

In the heterogeneous hydraulic conductivity scenario (the distributed K model), we observed that the groundwater heads were highest in the topographical hill (model grid row 25–30, Fig. 10) than in the other two model scenarios; uniform low K and uniform high K, even though the portion of the domain has a mainly high hydraulic conductivity. This happened because the area, after the model grid row 50 had low hydraulic conductivity and lateral flow velocity, decreased substantially and hindered the water flow from the high elevation to the low elevation. Another interesting phenomenon that occurred, was the pooling of groundwater at the boundary of low and high hydraulic conductivity regions (model grid row 51, Fig. 10), which was evident from the increase in groundwater heads to the drain level at model grid row 51. This increase in groundwater heads can be confirmed from the high DF value (DF=2). The increase in heads and pooling of water could be associated with the hindrance of water to move due to changes in the hydraulic conductivity zone, despite the steep slope (from west to east, between model grid row 50–53). Consequently, groundwater heads are unusually higher at the higher elevation of high hydraulic conductivity regions (see Fig. 11). Moreover, in the low hydraulic conductivity region (model grid row 52–68, Fig. 10), we consistently observed a DF range close to 1 while in the high hydraulic conductivity region the DF range was from 0.2 to 2. From these results we inferred that introduction of heterogeneity can disrupt the field scale lateral groundwater flows and result in excessive pooling of water on the boundaries of high and low hydraulic conductivities.

Due to these reasons, the TPI has no linear correlation with the DF in the distributed K model scenario. It appears that two distinct correlations exist with the TPI in the distributed K model scenario indicating a more complex preferential flow system (Fig. 9). Therefore, geology is important in the DF spatial distributions, that were underrepresented in uniform low K and uniform high K.

Past studies have conducted correlation analysis between the groundwater table and topographic characteristics (peaks and depressions) with respect to hydraulic conductivity on regional and continental scales (Condon and Maxwell, 2015; Gleeson and Manning, 2008). We expected some similarity in the correlation analysis between the tile drain flows and the relative topography of the current study. At a continental scale, Condon and Maxwell (2015) found a linear correlation only between water table depth and steep topography (major peaks and depressions) in high hydraulic conductivity and arid regions. However, at field scale, we found contrasting results. Topographic highs and lows, regardless of their steepness, showed a linear correlation in both high and low hydraulic conductivities with a slightly stronger correlation in the low hydraulic conductivity regions. The discrepancies between the continental-scale study and our field-scale study could be attributed to several factors, such as scale-dependent processes, hydrological connectivity, and variability in hydraulic conductivity.

Gleeson and Manning (2008) and Condon and Maxwell (2015) determined that the relationship between topography and groundwater table depth deviates from linearity when geological heterogeneity is considered. In this study we did not compare groundwater heads with TPI, however, the comparison of TPI and DF showed intermediate correlation suggesting that TPI can only be used for linear prediction of the DF in homogenous hydraulic conductivity areas and not heterogeneous hydraulic conductivity areas, unless the analysis is carried out separately for each hydraulic conductivity region.

4.7. Limitations of groundwater modelling technique

We observed that the DF produced by different geological models show a different spatial distribution (Fig. 7). One can argue about the accuracy of the developed model based on two limitations. First, previous studies have emphasized the importance of the impact of groundwater heads on tile drain flow generation (Boico et al., 2022), and calibration of the model results to known groundwater heads could have improved the predictive use of the model. Second, the groundwater model did not incorporate tile drainage parameters in the calibration that could have enhanced the model accuracy, given that drain conductance is influenced by the hydraulic conductivity of the surrounding geological deposits. However, the primary aim of the study was to obtain a comprehensive understanding of how geological heterogeneity affects the spatial distribution of tile drain flows rather than developing an accurate predictive model. Moreover, we developed simplified groundwater models to achieve the main objective and to avoid adding unnecessary complexity to the models.

In essence, this study uniquely addressed spatial patterns of tile drain flows, considering the unexplored influences of topography and geology, whereas, prior studies primarily examined the recharge to hydraulic conductivity ratio to discern if a groundwater system is recharge or topography controlled (Anderson et al., 2015; Haitjema and Mitchell-Bruker, 2005). The study presented simplified

groundwater models, where recharge was applied as main input and tile drainage was applied as a main output. Despite the topographical control on the spatial distribution of DF, geological heterogeneity exhibited varied effects on the spatial distribution of both DF and groundwater heads. In Uniform low K, discharge was relatively uniform across peaks and depressions, whereas in uniform high K, depressions had higher discharge and hills had lower discharge. Conversely, the distributed K model exhibited water pooling at the transition zone between high and low hydraulic conductivity, resulting in higher discharge at the zone boundaries. The findings suggested that the uniform low K and distributed K models were predominantly controlled by topography, in contrast to the uniform high K model, which was influenced by a combination of recharge and topography. Overall, this study highlighted the influence of small-scale geological variations on the spatial distribution of drain flows which are often underrepresented and not considered due to the lack of detailed geological information.

5. Conclusions

In conclusion, our study has taken a significant step in addressing the challenges of geological heterogeneity in groundwater modelling. We successfully captured the geological heterogeneity of the field by integrating 3D geophysical data with hydraulic conductivity estimates. We demonstrated that developing site-specific relationships between hydraulic conductivity and electrical resistivity, as well as using distinct resistivity thresholds for 3D groundwater modeling, holds promise for incorporating geological models into groundwater model simulations.

We concluded that the TPI predicts the high and low tile drainage discharge regions while hydraulic conductivity decides the magnitude of the tile drain flow in regions with homogeneous hydraulic conductivity, especially in clayey moraine landscape. Moreover, we demonstrated that heterogeneous hydraulic conductivity does not show a strong direct relationship with the TPI and depicts complex preferential flow behavior. That is why, in heterogeneous soils, the delineation of high and low hydraulic conductivities within the field is useful if the aim is to study the spatial distribution of tile drain flows.

The results of our study could be beneficial for water managers to spatially partition groundwater recharge and surface water fluxes. Understanding the association of topography-geology interaction and the spatial patterns of tile drain flow at a small-scale (10 m) will likely be critical as water managers move toward a more spatially differentiated understanding of the hydrological system. While our work focused on a relatively homogeneous clayey moraine landscape, the principles are applicable to other landscape types.

Overall, our research underscores the importance of comprehending local topography-geology interactions to accurately characterize the factors controlling tile drainage discharge. Knowledge of the groundwater flow system and the range of possible topography-geology interactions will narrow the uncertainty and give bounds for what can be expected from the system. Although it is encouraging that the groundwater system can be simulated numerically (giving rise to quantitative predictions throughout the watershed), more information regarding the controlling processes (such as spatial groundwater head distribution) that link topography-geology interaction to the DF is needed to attain truly integrated watershed management. This 'landscape' understanding of the system will likely become important as society demands more quantitative and spatially distributed answers from watershed managers.

CRediT authorship contribution statement

Hafsa Mahmood: Conceptualization, Methodology, Software, Formal analysis, Investigation, Writing-original draft, Visualization, Validation. **Rasmus Rumph Frederiksen:** Conceptualization, Methodology, Investigation, Formal analysis, Software, Visualization, Writing - review & editing, Supervision. **Anders Vest Christiansen:** Review & editing, Supervision. **Carlos Duque**: Review & editing, Supervision.

Declaration of Competing Interest

The authors declare that they have no known competing financial interests or personal relationships that could have appeared to influence the work reported in this paper.

Data Availability

Data will be made available on request.

Acknowledgements

This study was part of T-Rex project (Terrænnær redox og retentions-kortlægning til differentieret målrettet virkemiddelindsats indenfor ID15 oplande), funded by the Danish GUDP (Grønt Udviklings- og Demonstrationsprogram), project number 34009–18-1453 and WATEC – Aarhus University Center for Water Technology in Denmark. Authors would also like to thank Simon Stisen and Raphael Schneider for productive discussions and for sharing their knowledge of Ostrich calibration. Authors would also like to thank Niels Claes and Jesper Bjergsted Pedersen for helping with the geophysical data collection and modelling respectively. Lastly, authors would also like to thank Karen Engell Dalsgaard and Paul Jack McLachlan for helping with proofreading the Manuscript.

References

Anderson, M.P., Woessner, W.W., Hunt, R.J., 2015. Applied Groundwater Modeling: Simulation of Flow and Advective Transport. Elsevier,. https://doi.org/10.1016/C2009-0-21563-7.

Asadzadeh, M., Tolson, B., 2013. Pareto archived dynamically dimensioned search with hypervolume-based selection for multi-objective optimization. Eng. Optim. 45 (12), 1489–1509. https://doi.org/10.1080/0305215x.2012.748046.

Atkinson, P.M., & Lloyd, C.D. (2010). *geoENV VII – Geostatistics for Environmental Applications*.

Auken, E., Foged, N., Larsen, J.J., Lassen, K.V.T., Maurya, P.K., Dath, S.M., & Eiskjær, T. (2018b). tTEM reference - A Towed TEM system for Detailed 3D Imaging of the Top 70 meters of the Subsurface. *GEOPHYSICS*.

Auken, E., Foged, N., Larsen, J., Lassen, K., Maurya, P., Dath, S., Eiskjær, T., 2018a. tTEM – a towed TEM-system for detailed 3D imaging of the top 70 meters of the subsurface. Geophysics 84, 37. https://doi.org/10.1190/geo2018-0355.1.

Boico, V.F., Therrien, R., Højberg, A.L., Iversen, B.I., Koganti, T., Varvaris, T., 2022. Using depth specific electrical conductivity estimates to improve hydrological simulations in a heterogeneous tile-drained field. J. Hydrol. 604 https://doi.org/10.1016/j.jhydrol.2021.127232.

Boland-Brien, S.J., Basu, N.B., Schilling, K.E., 2014. Homogenization of spatial patterns of hydrologic response in artificially drained agricultural catchments. Sep 15 Hydrol. Process. 28 (19), 5010–5020. https://doi.org/10.1002/hyp.9967.

Cheremisinoff, N.P., 1998. Groundwater Remediation and Treatment Technologies. William Andrew Inc,.

Christiansen, A.V., Pedersen, J.B., Auken, E., Soe, N.E., Holst, M.K., Kristiansen, S.M., 2016. Improved geoarchaeological mapping with electromagnetic induction instruments from dedicated processing and inversion. Remote Sens. 8 (12). <Go to ISI>://WOS:000392489400051.

Clement, D.R., Steinman, A.D., 2017. Phosphorus loading and ecological impacts from agricultural tile drains in a west Michigan watershed. J. Gt. Lakes Res. 43 (1), 50–58. https://doi.org/10.1016/j.jglr.2016.10.016.

Condon, L.E., Maxwell, R.M., 2015. Evaluating the relationship between topography and groundwater using outputs from a continental-scale integrated hydrology model. Water Resour. Res. 51 (8), 6602–6621. https://doi.org/10.1002/2014wr016774.

Daly, C., Caers, J., 2010. Multi-point geostatistics – an introductory overview (https://doi.org/DOI:). EAGE 28 (9). https://doi.org/10.3997/1365-2397.2010020.

De Schepper, G., Therrien, R., Refsgaard, J.C., He, X., Kjaergaard, C., & Iversen, B.V. (2017, May). Simulating seasonal variations of tile drainage discharge in an agricultural catchment. *Water Resources Research*, *53*(5), 3896–3920. <Go to ISI>://WOS:000403712100024.

DUALEM-INC. (2021). *DualEM-421s* Dualem. Retrieved 12–03-2021 from to www. Dualem.com.

Frederiksen, R.R., Christiansen, A.V., Christensen, S., Rasmussen, K.R., 2017. A direct comparison of EMI data and borehole data on a 1000 ha data set. Geoderma 303, 188–195.

Frederiksen, R.R., Larsen, S.E., Mathiesen, G.B., & Kronvang, B. (2023). Development and application of a parsimonious statistical model to predict tile flow in minerogenic soils. *Agricultural Water Management*.

Gallant, J.C., Wilson, J.P., 2000. Primary topographic attributes. Terrain Analysis: Principles and Applications. Wiley,, New York, pp. 51–85.

Gleeson, T., Manning, A.H., 2008. Regional groundwater flow in mountainous terrain: three-dimensional simulations of topographic and hydrogeologic controls. Water Resour. Res. 44 (10) https://doi.org/ArtnW1040310.1029/2008wr006848.

Haitjema, H.M., Mitchell-Bruker, S., 2005. Are water tables a subdued replica of the topography? (Nov-Dec). Ground Water 43 (6), 781–786. https://doi.org/10.1111/j.1745-6584.2005.00090.x.

Hansen, A.L., Storgaard, A., He, X., Hojberg, A.L., Refsgaard, J.C., Iversen, B.V., & Kjaergaard, C. (2019a, Jan 30). Importance of geological information for assessing drain flow in a Danish till landscape. *Hydrological Processes*, *33*(3), 450–462. <Go to ISI>://WOS:000456206300010.

Hansen, A.L., Refsgaard, J.C., Christensen, B.S.B., Jensen, K.H., 2013. Importance of including small-scale tile drain discharge in the calibration of a coupled groundwater-surface water catchment model (https://doi.org/https://doi.org/). Water Resour. Res.. https://doi.org/10.1029/2011WR011783.

Hansen, A.L., Jakobsen, R., Refsgaard, J.C., Hojberg, A.L., Iversen, B.V., Kjaergaard, C., 2019b. Groundwater dynamics and effect of tile drainage on water flow across the redox interface in a Danish Weichsel till area. Adv. Water Resour. 123, 23–39. <Go to ISI>://WOS:000453714000003.

Heath, R.C. (1983). Basic ground-water hydrology. *Water-Supply Paper*.

Helmers, M.J., Abendroth, L., Reinhart, B., Chighladze, G., Pease, L., Bowling, L., Youssef, M., Ghane, E., Ahiablame, L., Brown, L., Fausey, N., Frankenberger, J., Jaynes, D., King, K., Kladivko, E., Nelson, K., Strock, J., 2022. Impact of controlled drainage on subsurface drain flow and nitrate load: A synthesis of studies across the US Midwest and Southeast. https://doi.org/ARTN 107265. Agric. Water Manag. 259 https://doi.org/10.1016/j.agwat.2021.107265.

Johnson, A.I. (1967). *Specific Yield - Compilation of Specific Yields for Various Materials*.

Kessler, T.C., Klint, K.E.S., Nilsson, B., Bjerg, P.L., 2012. Characterization of sand lenses embedded in tills. Quat. Sci. Rev. 53, 55–71. https://doi.org/10.1016/j.quascirev.2012.08.011.

Kladivko, E.J., Bowling, L.C., 2021. Long-term impacts of drain spacing, crop management, and weather on nitrate leaching to subsurface drains. J. Environ. Qual. 50 (3), 627–638. https://doi.org/10.1002/jeq2.20215.

Kladivko, E.J., Frankenberger, J.R., Jaynes, D.B., Meek, D.W., Jenkinson, B.J., Fausey, N.R., 2004. Nitrate leaching to subsurface drains as affected by drain spacing and changes in crop production system (https://doi.org/DOI). J. Environ. Qual. 33 (5), 1803–1813. https://doi.org/10.2134/jeq2004.1803.

Langevin, C.D., Hughes, J.D., Banta, E.R., Niswonger, R.G., Panday, S., & Provost, A.M. (2017). *Documentation for the MODFLOW 6 Groundwater Flow Model: U.S. Geological Survey Techniques and Methods* (Vol. A55). https://doi.org/https://doi.org/10.3133/tm6A55.

Mahmood, H., Schneider, R.M., Frederiksen, R.R., Christiansen, A.V., Stisen, S., 2023. Using jointly calibrated fine-scale drain models across Denmark to assess the influence of physical variables on spatial drain flow patterns. J. Hydrol.: Reg. Stud. 46, 101353 https://doi.org/10.1016/j.ejrh.2023.101353.

Mariethoz, G., Renard, P., & Straubhaar, J. (2010). The Direct Sampling method to perform multiple-point geostatistical simulations. https://doi.org/https://doi.org/10.1029/2008WR007621.

Matott, L. (2017). *OSTRICH: An Optimization Software Tool, Documentation and User's Guide Version 17.12.19*. In University at Buffalo Center for Computational Research. http://www.civil.uwaterloo.ca/envmodelling/Ostrich.html.

Mattivi, P., Franci, F., Lambertini, A., Bitelli, G., 2019. TWI computation: a comparison of different open source GISs. Open geospatial data. Softw. Stand 6, 4.

McNeill, J.D. (1980). Electromagnetic terrain conductivity measurement at low induction numbers. Technical Note TN-6. *Geonics Ltd*.

Motarjemi, S.K., Moller, A.B., Plauborg, F., Iversen, B.V., 2021. Predicting national-scale tile drainage discharge in Denmark using machine learning algorithms. J. Hydrol. -Reg. Stud. 36 https://doi.org/10.1016/j.ejrh.2021.100839.

Nielsen, J.A. (2015). DANSK MARKDRÆNINGSGUIDE.

Nilsson, B., Sidle, R.C., Klint, K.E., Boggild, C.E., Broholm, K., 2001. Mass transport and scale-dependent hydraulic tests in a heterogeneous glacial till-sandy aquifer system (https://doi.org/Doi). J. Hydrol. 243 (3–4), 162–179. https://doi.org/10.1016/S0022-1694(00)00416-9.

Olesen, J.E., & Heidmann, T. (2002). EVACROP: Et program til beregning af aktuel fordampning og afstrømning fra rodzonen.

Remy, N., 2005. S-GeMS: the stanford geostatistical modeling software: a tool for new algorithms development. Geostatistics Banff 2004. Springer,, Dordrecht, pp. 865–871.

Ross, J.A., Herbert, M.E., Sowa, S.P., Frankenberger, J.R., King, K.W., Christopher, S.F., Tank, J.L., Arnold, J.G., White, M.J., Yen, H., 2016. A synthesis and comparative evaluation of factors influencing the effectiveness of drainage water management. Agric. Water Manag. 178, 366–376. https://doi.org/10.1016/j.agwat.2016.10.011.

Schilling, K.E., Jindal, P., Basu, N.B., Helmers, M.J., 2012. Impact of artificial subsurface drainage on groundwater travel times and baseflow discharge in an agricultural watershed, Iowa (USA). Hydrol. Process. 26 (20), 3092–3100. https://doi.org/10.1002/hyp.8337.

Schilling, K.E., Gassman, P.W., Arenas-Amado, A., Jones, C.S., Arnold, J., 2019. Quantifying the contribution of tile drainage to basin-scale water yield using analytical and numerical models. Sci. Total Environ. 657, 297–309. https://doi.org/10.1016/j.scitotenv.2018.11.340.

Schilling, K.E., Streeter, M.T., Vogelgesang, J., Jones, C.S., Seeman, A., 2020. Subsurface nutrient export from a cropped field to an agricultural stream: implications for targeting edge-of-field practices. https://doi.org/ARTN 106339 Agric. Water Manag. 241. https://doi.org/10.1016/j.agwat.2020.106339.

Schwartz, F.W., & Zhang, H. (2003). Fundamentals of Ground Water. Wiley. (Wiley).
Sinai, G., Jain, P.K., 2005. Water management of irrigated-drained fields in the Jordan Valley South of Lake Kinneret (https://doi.org/Doi). J. Irrig. Drain. Eng. 131 (4), 364–374. https://doi.org/10.1061/(Asce)0733-9437(2005)131:4(364).
Sloan, B.P., Mantilla, R., Fonley, M., Basu, N.B., 2017. Hydrologic impacts of subsurface drainage from the field to watershed scale. Hydrol. Process. https://doi.org/10.1002/hyp.11218.
Varvaris, I., Børgesen, C.D., Kjærgaard, C., Iversen, B.V., 2018. Three two-dimensional approaches for simulating the water flow dynamics in a heterogeneous tile-drained agricultural field in Denmark. Soil Sci. Soc. Am. J. 82, 1367–1383. https://doi.org/10.2136/sssaj2018.05.0190.
Viezzoli, A., Auken, E., Munday, T., 2009. Spatially constrained inversion for quasi 3D modelling of airborne electromagnetic data – an application for environmental assessment in the Lower Murray Region of South Australia. Explor. Geophys. 40.
Vignoli, G., Fiandaca, G., Christiansen, A.V., Kirkegaard, C., Auken, E., 2015. Sharp spatially constrained inversion with applications to transient electromagnetic data. Geophys. Prospect. https://doi.org/10.1111/1365-2478.12185.
Voss, C.I., 2011. Editor's message: groundwater modeling fantasies —part 1, adrift in the details. Hydrogeol. J. 19.
Williamson, R.E., Kriz, G.J., 1970. Response of agricultural crops to flooding, depth of watertable, and soil gaseous composition. Trans. ASAE 13, 216–220.
Zucker, L.A., Brown, L.C., 1998. Agricultural drainage: water quality impacts and subsurface drainage studies in the midwest. Ohio State Univ. Ext. Bull. 871.